



Contents lists available at ScienceDirect

Journal of Controlled Release

journal homepage: [www.elsevier.com/locate/jconrel](http://www.elsevier.com/locate/jconrel)

## Distal phenylalanine modification for enhancing cellular delivery of fluorophores, proteins and quantum dots by cell penetrating peptides

E.J. Sayers<sup>a,1</sup>, K. Cleal<sup>b,1</sup>, N.G. Eissa<sup>a,c</sup>, P. Watson<sup>b</sup>, A.T. Jones<sup>a,\*</sup>

<sup>a</sup> Cardiff School of Pharmacy and Pharmaceutical Sciences, Redwood Building, Cardiff University, Cardiff, Wales CF10 3NB, UK

<sup>b</sup> Cardiff School of Biosciences, Cardiff University, Cardiff, Wales CF10 3AX, UK

<sup>c</sup> Department of Pharmaceutics, Faculty of Pharmacy, Zagazig University, Zagazig 44519, Egypt

### ARTICLE INFO

#### Article history:

Received 15 April 2014

Accepted 29 July 2014

Available online xxxxx

#### Keywords:

Bovine serum albumin  
Cell penetrating peptides  
CPP  
Quantum dots  
Phenylalanine  
Protein delivery

### ABSTRACT

For cell penetrating peptides (CPPs) to fulfil their promise as effective delivery vectors we need a better understanding of their mechanisms of cell binding and uptake. This is especially the case when they are linked to different types of cargo. Here we describe new studies based on our previous findings suggesting that, for peptide-CPP chimeras, distal hydrophobic residues upstream of the CPP sequence can have profound effects on the way they interact with cells. We studied peptides bearing an N-terminal Glycine or Phenylalanine linked via a neutral and flexible bridging group, SGSGSGSG, to three well-studied CPPs: octaarginine, penetratin and TP10. Using a combination of flow cytometry, live-cell imaging and image analysis we examined the effects of this single amino acid change on binding and uptake of Alexa488-fluorophore, bovine serum albumin and quantum dot cargoes. The influence of the glycine–phenylalanine switch for fluorophore delivery was most dramatic in TP10, increasing cellular uptake by 4.4 and 9.9 fold in non-adherent and adherent cells, respectively. Only penetratin showed effective uptake of bovine serum albumin with the phenylalanine variant showing an increase of 1.6 fold over the glycine variant. The uptake of quantum dots was most efficiently demonstrated by octaarginine, with the glycine variant increasing uptake 4.8 fold and the phenylalanine variant increasing uptake 9.5 fold over quantum dots alone. Overall the data demonstrate that hydrophobicity distal to the CPP could be utilised to enhance their capacity to bind to the cell membrane and deliver a range of macromolecules to the insides of cells.

© 2014 The Authors. Published by Elsevier B.V. This is an open access article under the CC BY license (<http://creativecommons.org/licenses/by/3.0/>).

### 1. Introduction

Cell penetrating peptides (CPPs) have been extensively explored as potential delivery mechanisms for biopharmaceuticals such as peptides, proteins or nucleic acids (reviewed here [1]). Cargo can be associated with CPPs via different mechanisms for example through extension of the CPP sequence at the N or C-terminus, through a chemical link to a side chain such as cysteine, or the CPPs can associate via an ionic or hydrophobic interaction with a cargo. For highly charged cationic CPPs such as R8 and Tat there is also clear evidence that they bind with serum proteins which can affect both their stability and internalisation capacity [2]. Via a similar mechanism CPPs can be utilised to bind to specific proteins to deliver them into different cell types [3]. This has significant potential in the delivery of biopharmaceuticals, and has expanded

into *in vivo* studies with one notable example being the CPP penetratin being explored as a potential delivery mechanism for insulin [4].

CPPs have also been shown to deliver a range of metallic nanoparticles (NPs) into cells [5]. Quantum dots (Qdots) are small, ~10–25 nm, fluorescent nanocrystals that have received much attention due to their unique spectral and chemical characteristics. Qdots offer many advantages over standard fluorescent proteins and small molecules especially with respects to their attractive luminosity and photostability properties that allow for long-term visualisation of cellular structures and events, with the potential to discriminate individual particles for single particle tracking experiments [6–8]. Accordingly, Qdots are increasingly deployed as intracellular live-cell probes and are also expected to find use in medical diagnostics for example as contrast agents. Recently a cysteine–histidine rich nona-arginine peptide (C-5H-R9-5H-C) was designed with the aim of enhancing Qdot uptake through modification of the net hydrophobicity of the peptide to promote membrane association [9]. Although the peptide enhanced Qdot uptake at high nanoparticle concentrations (100 nM Qdots complexed with 6 μM peptide) over R9 alone or Pas (FFLIP) modified R9, a direct translocation of the complex through the plasma membrane was cited as the major route of entry due to the accumulation of material within cells at 4 °C [9].

\* Corresponding author at: Cardiff School of Pharmacy and Pharmaceutical Sciences, Redwood Building, Cardiff University, Cardiff, CF10 3NB, Wales, UK. Tel.: +44 2920876431; fax: +44 2920874536.

E-mail address: [jonesat@cardiff.ac.uk](mailto:jonesat@cardiff.ac.uk) (A.T. Jones).

<sup>1</sup> Both authors contributed equally to this work.

To date only a relatively small number of the hundreds of defined CPP sequences have been extensively studied with respect to their interaction with cells and cellular uptake. Modifications in residues within the CPP at single amino acid level have been demonstrated to significantly affect cell uptake, however, much less attention has been given to the effect the cargo may have on CPP delivery capacity [10]. The same can be said for relatively small cargo such as short peptide sequences. Indeed, a particularly attractive goal in drug delivery research, targeting a number of diseases, is to identify a CPP that could deliver a therapeutic peptide, either by direct plasma membrane translocation, or endocytosis to the interior of the cell to specifically interfere with a protein–protein interaction to modify cellular physiology. There is a wealth of CPP literature on this subject but very few have directed research effort to cargo effects. Recently we discovered that a single hydrophobic residue change (Ala/Phe) at the N-terminus of a 9-residue cargo sequence had a dramatic effect on the cellular interaction and the mechanism of cell death of the Bcl-2 converter peptide D-NuBCP-9-r8 (fsrslhslIG-Ahx-rrrrrrrr) [11].

Here we extend on these findings to study the effects of exchanging a single Gly residue to a Phe at the N-terminus of a commonly utilised hydrophilic linker [12] (GSGSGSGSG) versus (FSGSGSGSG) attached at the N-terminal end of well-characterised CPPs, octaarginine, TP10 and penetratin. We demonstrate that this single residue change has, in some cases, striking effects on CPP cell binding and capacity to deliver fluorophores, proteins and Qdots into cells.

## 2. Materials and methods

### 2.1. Materials

Cell culture media, serum, trypsin, Hoechst 33342, Alexa Fluor 488 C5-maleimide, bovine serum albumin (BSA)–Alexa647, 10 kDa dextran–Alexa647 and Qdots (Qdot® 655 ITK™ Amino (PEG)) were purchased from Life Technologies (Paisley, UK). Heparin sulphate, Concanavalin A-FITC and sodium HEPES were purchased from Sigma Aldrich (Gillingham, UK).

### 2.2. Cell culture

HeLa, human cervical carcinoma, cells (EMBL, Heidelberg, Germany) were maintained in a humidified 5% CO<sub>2</sub> 37 °C incubator as a subconfluent monolayer in DMEM supplemented with 10% foetal bovine serum. Human acute myeloid leukaemia KG1a cells (ECACC, Porton Down, UK) were maintained at a confluency of between 0.5 and 2 × 10<sup>6</sup> cells/mL in RPMI 1640 medium supplemented with 10% foetal bovine serum.

### 2.3. Peptide labelling

All peptides were purchased, unlabelled, from EZBiolabs, Carmel USA (listed in Table 1) and labelled using Alexa 488 maleimide based on minor modifications of a previously described method [13]. Briefly, peptides were dissolved in methanol at a concentration of 2 mg/mL

and reacted with Alexa 488 C5-maleimide (also dissolved in methanol to 2 mg/mL) at a molar ratio of 1.1 to 1 peptide/fluorophore for 3 h at room temperature. Labelled peptides and reactants were separated using reverse phase HPLC on a C18 Luna 100 Å 5-µm semipreparative column (Phenomenex, Macclesfield, UK) with the labelled peptide collected and freeze-dried. Labelling and conjugate mass was confirmed by matrix-assisted laser-desorption ionisation–time-of-flight spectrometry and quantified by UV spectrometry. All labelled peptides were resuspended to a stock concentration of 1 mM in autoclaved distilled water, aliquoted and frozen at –80 °C until needed.

### 2.4. Flow cytometry analysis

HeLa cells were seeded at a density of 1 × 10<sup>5</sup> cells per well the day before the experiment in a 12-well plate. On the day, cells were incubated with 2 or 5 µM labelled peptide in complete medium for 1 h in a 37 °C 5% CO<sub>2</sub> incubator before trypsinisation in 0.05% Trypsin–EDTA for 5 min. KG1a cells were seeded into a 12-well plate at a density of 2 × 10<sup>5</sup> cells per well and incubated with 2 or 5 µM of labelled peptide in complete medium for 1 h in a 37 °C 5% CO<sub>2</sub> incubator. Both trypsinised HeLa cells and suspension KG1a cells were washed by centrifugation (800 ×g for 2 min) at 4 °C in ice cold PBS before washing in ice cold 140 µg/mL heparin sulphate in PBS to remove surface bound peptide and washed a further three times in ice cold PBS. Samples were analysed on a Becton Dickinson FACSCalibur analyser, gated using forward and side scatter with 1 × 10<sup>4</sup> viable cells analysed. Statistical significance was tested using a one-way ANOVA test.

### 2.5. Cell binding and uptake analysis using confocal microscopy

HeLa cells were seeded at a density of 2.5 × 10<sup>5</sup> cells per imaging dish (MatTek, Ashland, US) and allowed to adhere overnight under tissue culture conditions. On the day of experiment, cells were incubated with 2 or 5 µM labelled peptide and incubated for 1 h, 37 °C 5% CO<sub>2</sub>. Cells were washed in PBS followed by 140 µg/mL heparin sulphate in PBS and finally imaged in imaging medium (phenol red free DMEM supplemented with 10% FBS and 20 mM HEPES) on a Leica SP5 confocal microscope (63× 1.4 NA objective using a 488 nm laser with a 95.5 µm pinhole, pixel size is 283 nm, using Leica Type F immersion oil).

KG1a cells were incubated in 200 µL complete medium containing either 2 or 5 µM labelled peptide at a density of 1 × 10<sup>5</sup> cells per well for 1 h under tissue culture conditions. Cells were washed in PBS and heparin followed by centrifugation (as for flow cytometry above) and immediately imaged in imaging medium as above. Microscopy and processing settings were kept consistent within each set of CPPs.

### 2.6. Pulse chase analysis of F-/G-(SG)<sub>4</sub>TP10-Alexa488

In a 35 mm imaging dish 1.75 × 10<sup>5</sup> cells were seeded in complete medium and allowed to adhere overnight in a 37 °C incubator. On the morning of the experiment 200 µg/mL 10 kDa dextran–Alexa647 was pulsed into the cells for 2 h in complete medium before washing and allowed to internalise by chasing for a further 4 h in complete medium.

**Table 1.**

Names and sequences of the peptides used in this study. All peptides use L-amino acids, bold letters denote the changed hydrophobic - neutral amino acid, D-amino acids are lower case and cell penetrating peptide sequences are underlined. Net charge, hydrophobicity and pI were calculated using Biosynthesis' Peptide Properties calculator.

Peptide	Sequence	Net charge (pH 7)	Hydrophobicity (pH 6.8)	pI
F(SG) <sub>4</sub> R8	Ac-FSGSGSGSGRRRRRRRRCG-NH <sub>2</sub>	7.91	0.74	13.53
G(SG) <sub>4</sub> R8	Ac-GSGSGSGSGRRRRRRRRCG-NH <sub>2</sub>	7.91	–4.37	13.53
F(SG) <sub>4</sub> Pen	Ac-FSGSGSGSGRQIKIWFQNRRMKWKKGC-NH <sub>2</sub>	6.91	18.3	12.83
G(SG) <sub>4</sub> Pen	Ac-GSGSGSGSGRQIKIWFQNRRMKWKKGC-NH <sub>2</sub>	6.91	14.7	12.83
F(SG) <sub>4</sub> TP10	Ac-FSGSGSGSGAGYLLGKINLKALAALAKKILGC-NH <sub>2</sub>	3.91	33.09	10.66
G(SG) <sub>4</sub> TP10	Ac-GSGSGSGSGAGYLLGKINLKALAALAKKILGC-NH <sub>2</sub>	3.91	30.06	10.66
cRGD	cyclo (RGDFK)			

Cells were loaded with 2  $\mu\text{M}$  F-/G-(SG)<sub>4</sub>TP10-Alexa488 for 1 h in complete medium before washing and imaging on the confocal microscope as previously described, using the 488 nm and 633 nm lasers. The cells were subsequently returned to the 37 °C incubator before imaging 24 h after initial incubation with the peptide on the confocal microscope as previously described. For colocalization analysis individual cells were selected according to their DIC profile and analysed to obtain the mean unthresholded Pearson's coefficient per cell using the ImageJ plugin Coloc 2 for an average of 31 cells  $\pm$  3 for each experiment condition.

### 2.7. Peptide complexation with BSA–Alexa647

HeLa cells were seeded at a density of  $2.5 \times 10^5$  cells per imaging dish and allowed to adhere overnight under tissue culture conditions. Separately, 2  $\mu\text{M}$ , 500 nM or 100 nM of unlabelled peptide or peptide diluent control was incubated for 30 min with 2  $\mu\text{g}/\text{mL}$ , 500 ng/mL or 100 ng/mL BSA–Alexa647 respectively in autoclaved distilled 0.2  $\mu\text{m}$  filtered water in a final volume of 50  $\mu\text{L}$  at 37 °C. To this, 150  $\mu\text{L}$  of complete medium was added and incubated with the cells for 1 h, 37 °C 5% CO<sub>2</sub>. Cells were washed and imaged in imaging media (supplemented for the final 10 min with 10  $\mu\text{g}/\text{mL}$  Hoechst 33342) as described with microscopy settings remaining constant for all images for comparative CPP uptake analysis.

### 2.8. Peptide complexation with Qdots

For gel electrophoresis, 25 nM Qdots were complexed with 0.25  $\mu\text{M}$  to 250  $\mu\text{M}$  peptide for 30 min in PBS at room temperature. Products were assessed by gel electrophoresis on horizontal 0.8% agarose gels using TAE pH 8.0 running buffer. Sample (10  $\mu\text{L}$ ) was loaded with 3  $\mu\text{L}$  30% glycerol in running buffer and run for 1 h under a steady current and 100 V (4 V per 1 cm of gel).

### 2.9. Live-cell imaging of Qdot uptake

Qdot and peptide stocks were prepared separately at 100 $\times$  in PBS before combining in serum free DMEM for 30 min at RT and adding to cells at 37 °C. HeLa cells were seeded at  $1 \times 10^4$  cells per cm<sup>2</sup> in 96 well black walled plastic dishes (Greiner  $\mu\text{clear}$  Bio One, Stonehouse, UK), or glass coverslips and grown for 48 h in complete media. Cells were treated for 1 h in serum free DMEM before counterstaining with 25  $\mu\text{g}/\text{mL}$  Concanavalin A-FITC (ConA) for 5 min in serum free DMEM to label the plasma membrane. ConA treated cells were then washed a further 3 $\times$  in fully supplemented DMEM before immediate analysis as live cells by wide-field fluorescence microscopy or following a further 24 h incubation in complete media under tissue culture conditions. Cells were imaged using an Olympus (London, UK) wide-field imaging system (Olympus 20  $\times$  0.75 NA lens).

### 2.10. Quantification of Qdot uptake and colocalization analysis

Using ImageJ [14] an average of 66 individual cells (minimum of 51) were segmented based on ConA cell-surface stain profiles and analysed. A rolling ball background subtraction was performed (radius = 50) and untreated cells were used as baseline. Apoptotic and dividing cells identified by distinct morphological characteristics such as cellular blebs or the occurrence of a pair of rounded cells in close contact were discarded from analysis. For Qdot uptake analysis, the integrated intensity per cell was quantified per treatment condition. For colocalisation analysis individual cells were analysed to obtain the mean Pearson's coefficient per cell using the ImageJ plugin Coloc 2.

Tests for statistical equality were performed using a two tailed *t*-test assuming unequal variance.

## 3. Results and discussion

### 3.1. Fluorophore as CPP cargo

We have previously shown that a single N-terminal amino acid modification, spaced nine residues from the CPP octaarginine, from alanine to phenylalanine had a dramatic effect on its interaction with and uptake into cells [11]. It was therefore of interest to investigate what effect a single phenylalanine change distal to the CPP sequence would have on well-characterised CPPs octaarginine, penetratin and TP10 (Table 1) using a membrane impermeable sequence (SG)<sub>4</sub> that is frequently used as a bridging sequence in protein research [15].

After analysis by flow cytometry, KG1a cells showed a small but significant increase in uptake of octaarginine peptides F(SG)<sub>4</sub>R8-Alexa488 over G(SG)<sub>4</sub>R8-Alexa488 at 2  $\mu\text{M}$ , while HeLa cells showed no significant change at this concentration (Fig. 1a and c). At 5  $\mu\text{M}$  both cell types showed a small but significant increase in cell uptake of the Phe peptide over the Gly peptide (Fig. 1b and d). By microscopy, the difference in uptake is not as clearly visible at either concentration with the exception of KG1a at 5  $\mu\text{M}$  where some cells show cytosolic labelling in addition to the punctate labelling seen at the lower concentration (Fig. 2). We have previously shown there is a similarly heterogeneous population of cytosolic and punctate labelling in KG1a cells when incubated with 5  $\mu\text{M}$  R8-Alexa488 [16] indicating the capacity to enter the cytosol is not likely due to the phenylalanine alone.

Both penetratin and TP10 contain hydrophobic residues in their sequence to differing degrees (Table 1). Penetratin is classified as a cationic peptide, due to the high number of lysine and arginine amino acids present within its sequence, but also contains the hydrophobic amino acids isoleucine and phenylalanine [10]. TP10 is classified as an amphipathic CPP, it naturally forms into a helical structure displaying cationic residues on one side of the helix and hydrophobic residues on the other. These are likely to interact with cells in a different way compared to purely cationic CPPs and we investigated this further with the same cargo sequences.

Penetratin showed a >100% increase in the uptake of F(SG)<sub>4</sub>Pen-Alexa488 over G(SG)<sub>4</sub>Pen-Alexa488 in HeLa cells at both 2 (119%) and 5  $\mu\text{M}$  (164%) concentrations (Fig. 1c and d). Whilst in KG1a cells there was a significant increase at 5  $\mu\text{M}$  with a small but non-significant increase at 2  $\mu\text{M}$  (Fig. 1a and b). The influence of the Gly–Phe switch in

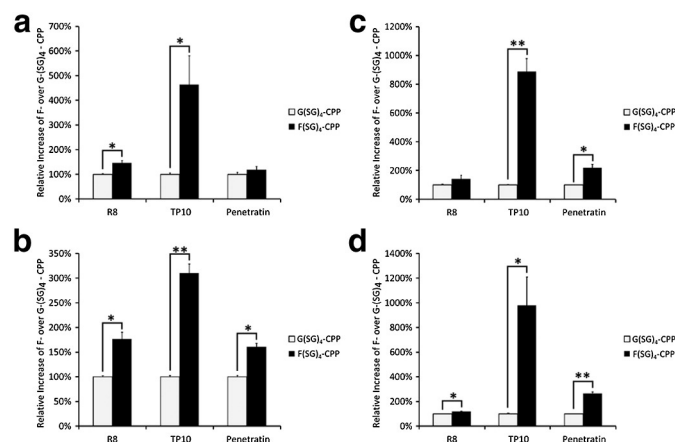


**Fig. 1.** Flow cytometry analysis of the uptake of 2 or 5  $\mu\text{M}$  Alexa488 labelled peptide into HeLa and KG1a cells. Graphs represent the increase in fluorescent intensity in response to the cellular uptake of either 2  $\mu\text{M}$  (a and c) or 5  $\mu\text{M}$  (b and d) of the peptides F(SG)<sub>4</sub>-R8/-TP10/-Pen-Alexa488 relative to the uptake of G(SG)<sub>4</sub>-R8/-TP10/-Pen-Alexa488 respectively. Uptake was measured after 1 h at 37 °C in complete medium in KG1a (a–b) or HeLa (c–d) cells and analysed by flow cytometry. Fluorescence intensity data is calculated using the geometric mean following three independent experiments performed in duplicate, error bars represent standard error. \* *p* < 0.05, \*\* *p* < 0.005. Sample Histograms are included as Supplementary Figure 1.

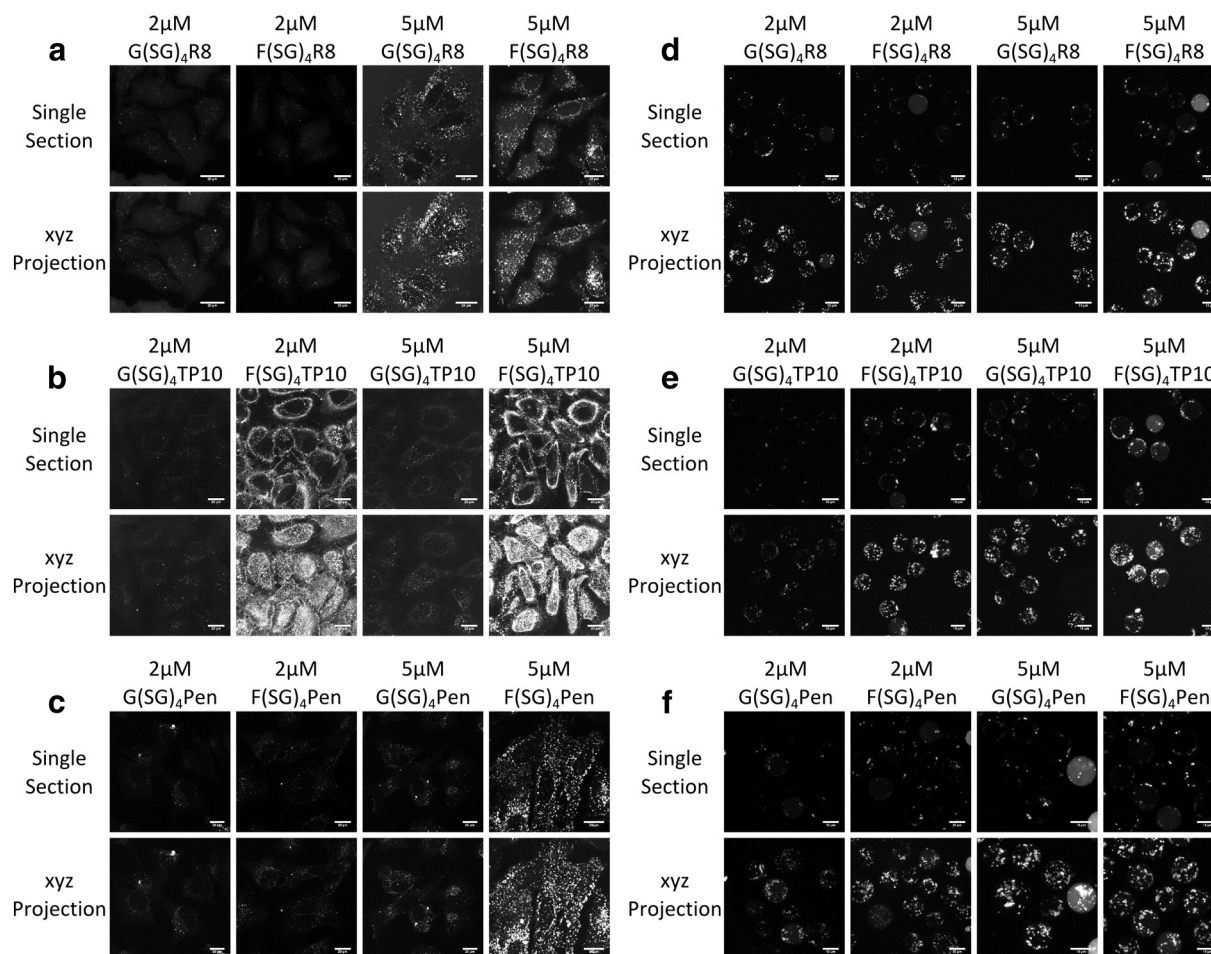


**Fig. 2.** Uptake of Alexa488 labelled peptides into HeLa and KG1a cells at 2 or 5  $\mu\text{M}$  after 1 h incubation in complete medium. Peptides, F-/G- (SG)<sub>4</sub>R8-Alexa488 (a, d), F-/G- (SG)<sub>4</sub>TP10-Alexa488 (b, e) or F-/G- (SG)<sub>4</sub>TP10-Alexa488 (c, f) at either 2 or 5  $\mu\text{M}$  were incubated in complete medium for 1 h at 37 °C with HeLa (a-c) or KG1a (d-f) cells and imaged immediately by confocal microscopy. Images represent either a single section through the cell at the mid-point of the nucleus, or maximum projections of the whole cell. Scale bar = 20  $\mu\text{m}$  (HeLa, a-c) or 10  $\mu\text{m}$  (KG1a, d-f).

TP10 was the most striking in both cell lines at both concentrations (Fig. 1). A likely reason for this considerable increase in HeLa cell fluorescence (~800%) was discovered when peptide uptake was viewed via microscopy that revealed extensive F(SG)<sub>4</sub>TP10-Alexa488 labelling of the plasma membrane that could account for this significant increase in cell associated fluorescence (Fig. 2). This membrane bound peptide did not, however, account for the total increase in signal as single section images also identified intracellular punctate structures indicating endocytosis. The fluorescence intensity of these structures were appreciably greater in the Phe over the Gly variant. Quantification of fluorescence uptake images of the TP10-Alexa488 variants confirms this with whole cell, membrane and intracellular fluorescence profiles all higher in the Phe variant over the Gly control (Supplementary Fig. 2), despite a large proportion of the peptide found on the plasma membrane. After further incubation of these cells in the absence of additional peptide addition this membrane fraction was significantly depleted (Fig. 3). Colocalisation analysis demonstrated that a large proportion of both the Phe and Gly variants of TP10 after this chase period colocalised with lysosomal dextran (Pearson's coefficient of  $0.85 \pm 0.07$  and  $0.72 \pm 0.08$  respectively). This value is significantly higher than that observed after 1 h where the vast majority of the peptide label is confined to the plasma membrane ( $0.42 \pm 0.08$  and  $0.47 \pm 0.09$  respectively). Quantification of the amount of total cell associated fluorescence at the end of the chase period indicates that the majority of the initial membrane associated fluorescence is internalised to lysosomes via membrane turnover. Interestingly, there was little evidence

of plasma membrane bound G(SG)<sub>4</sub>TP10-Alexa488 or F(SG)<sub>4</sub>TP10-Alexa488 in KG1a cells after identical one hour incubations (Fig. 2e) but revealed a much higher level of fluorescence for cells treated with the F variant, with 5  $\mu\text{M}$  peptide incubations resulting in some degree of cytosolic labelling.

Microscopy analysis revealed distinct punctate structures when visualising penetratin variants, with a clear increase in uptake of the Phe over the Gly form at 5  $\mu\text{M}$  in HeLa cells (Fig. 2) reflecting the change seen in the FACS data (Fig. 1). This difference is more difficult to visualise in KG1a cells with both forms of the peptide showing clear punctate structures and at 5  $\mu\text{M}$  both peptides demonstrating cytoplasmic labelling.

A number of studies have shown that direct hydrophobic modifications of CPPs show improved abilities to internalise into cells. A Phe-Phe addition to the N-terminus of octaarginine has been shown to greatly increase its internalisation, with the longer F<sub>4</sub> sequence increasing this further [17]. PasR8, which has the hydrophobic FFLIP sequence at the N-terminus of octaarginine, also aids octaarginine internalisation [18]. Increasing distal hydrophobicity via the Gly/Phe mechanism described had positive effects but these were modest for R8 compared with the other two CPPs. Our data therefore suggests that hydrophobicity within the CPP itself is an important parameter for enhancing uptake via this mechanism (Table 1). Penetratin requires the presence of a central tryptophan for membrane translocation [4], this residue is frequently found at the membrane-water interface in transmembrane proteins [19]. If the phenylalanine itself aids in membrane association it would be interesting to determine whether the effects of phenylalanine can

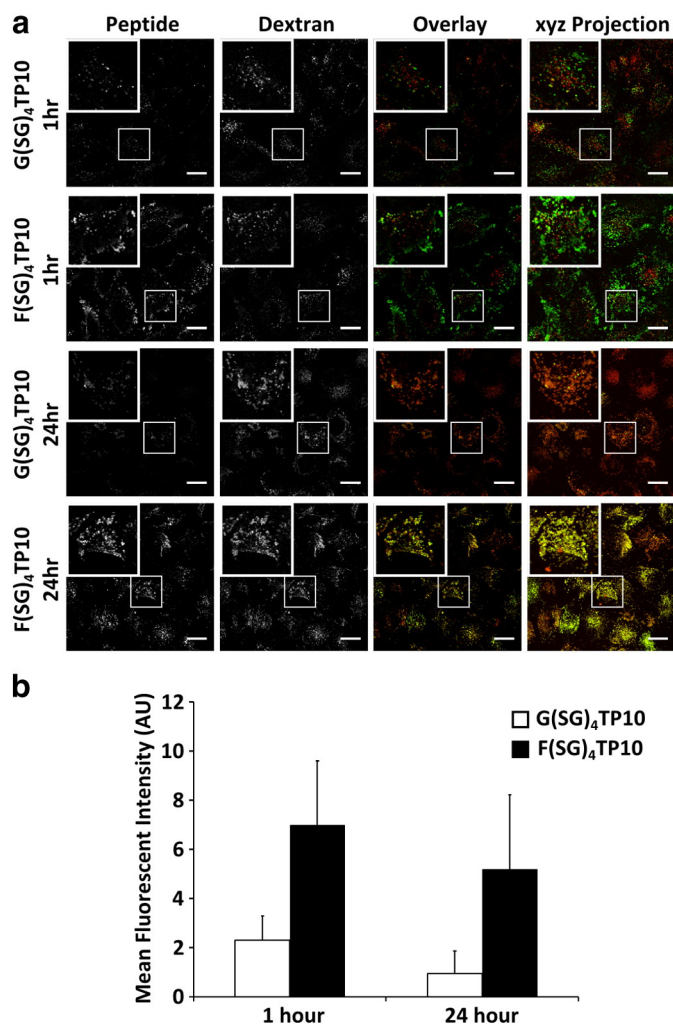


**Fig. 3.** Uptake and 24 h internalisation of F-/G-(SG)<sub>4</sub>TP10-Alexa488 into HeLa cells. HeLa cells were incubated with 2  $\mu$ M F- or G-(SG)<sub>4</sub>TP10-Alexa488 for 1 h before washing and imaging in complete imaging medium, the cells were then returned to the incubator and imaged after 24 h. (a) Images represent a single section taken on the confocal microscope of peptide (green) and pulse-chased dextran (red) with colocalisation as yellow. Scale bar = 20  $\mu$ m. Images were quantified for cell associated G- or F-(SG)<sub>4</sub>TP10-Alexa488. (b) Data represents the mean fluorescence intensity per cell of an average of 24  $\pm$  4 cells, error bars represent  $\pm$  SD.

be enhanced by Trp or whether these two amino acids together could have synergistic effects with respect to cell binding and translocation to the insides of cells.

### 3.2. Protein as CPP cargo

Penetratin, HIV-Tat, and transportan have previously been shown to be able to deliver BSA as non-covalent complexes into a range of cell lines [3]. Both HIV-Tat and transportan are closely related to the peptides used in this study, with the former being highly cationic, and TP10 being a shorter derivative of transportan. Based on our studies with a small fluorophore as cargo (Figs. 1–2) we investigated by live cell confocal microscopy, whether the Gly/Phe switch had any effect on the capacity of these peptides to deliver BSA.

Internalisation of BSA alone was barely detectable in HeLa cells at 0.5  $\mu$ g/mL and to visibly observe the uptake of this protein required increasing the concentration to 25  $\mu$ g/mL (Fig. 4). For TP10 and penetratin complexes, with BSA at a final concentration of 0.5  $\mu$ g/mL on cells both Gly and Phe variants increased uptake into distinct punctate endosomal structures. Of these peptides F(SG)<sub>4</sub>Pen showed the highest capacity to deliver BSA with an increase of 58% of the Phe over

the Gly variant (Supplementary Fig. 3). Both TP10 variants were able to deliver BSA into HeLa cells, however, the differences between these two with respects to BSA delivery capacity was small with a high degree of variance between cells. At lower complex concentrations both penetratin and TP10 BSA complexes continued to internalise into punctate structures visible above the background fluorescence (Supplementary Fig. 4) although there is a degree of variance between cells. There was no increase in the uptake of BSA by the two R8 variants, compared to BSA alone. This may be due to differences in BSA-complexation, cell interaction or stability. For all peptides and concentrations studied here, using this microscopy method, we could not detect diffuse BSA labelling over background fluorescence thus it remains to be determined whether any of the CPPs deliver proteins into the cytosol.

Albumin has a pI of 4.7 making it negatively charged in water [20], and CPP-peptides studied here all have a pI greater than 10 making them positively charged in the same solution. The preformed penetratin-/TP10-BSA complexes showed stability under the experimental conditions used that allowed for cell entry via endocytosis. Of note here is that all the peptides contain a free cysteine at the C-terminus and this reactive amino acid could have also contributed to aiding complexation to BSA and also plasma membrane binding [21].

### 3.3. Qdots as CPP cargo

Interaction of CPPs with anionic Qdots has been previously documented [22,23] and is thought to reflect electrostatic interactions between anionic groups on the nanoparticle surface, typically carboxyl groups as found in many commercial QD preparations, and basic arginines or lysines on the CPP. The specific display of a non-covalently bound CPP on the surface of a Qdot is expected to be critical in determining the interaction of the peptide with the cell membrane, and there is considerable scope for engineering a peptide which favourably interacts with both the nanoparticle and the cell surface.

Here, we further explored utilising non-covalent binding of CPPs as a paradigm for delivering anionic Qdots using our panel of Phe modified peptides. To assess binding, CPPs were complexed with Qdots and analysed by agarose gel electrophoresis. All CPPs used in this study formed complexes with the Qdots demonstrated by a reversal of Qdot migration, now towards the negative electrode (Fig. 5a). The migration of the entire panel of CPP:Qdot complexes is shown in Supplementary Fig. 5 and summarised in Fig. 5b. This is presented as the maximum migration of Qdot:CPP complexes, against Qdot alone towards the positive electrode. cRGD as a peptide with a small size and low net charge showed no evidence of binding. At higher CPP concentrations Qdot complexes progressively acquired a positive net charge, although for some peptides, particle aggregation was apparent due to the streaking of bands or the entrapment of material within the loading-well (Fig. 5, Supplementary Fig. 5). Aggregation was most clearly observed in G(SG)<sub>4</sub>TP10 treated Qdots which resulted in the formation of large aggregates which failed to migrate into the gel matrix. F(SG)<sub>4</sub>TP10 and Pen based peptides demonstrated streaking during migration implying the formation of heterogeneous aggregates at higher peptide concentrations. Particle aggregation is a critical parameter when preparing drug delivery complexes due to the potential wide-ranging effects resulting from this process [24,25]. Clear aggregation of Qdots when using G(SG)<sub>4</sub>TP10 could result from a particular orientation of the peptide at the Qdot surface which acts to destabilise the repulsive force between adjacent particles and promote agglomeration through either ionic or van der Waals modes [25]. For R8 based peptides, aggregation was not evident by gel electrophoresis (Fig. 5a) allowing for further cell-based analysis with these entities. Qdots by themselves demonstrated appreciable levels of binding to HeLa cells following a 1 h exposure in serum free media (Supplementary Fig. 6). Counterstaining with the lectin ConA to label the plasma membrane at the end of the experiment

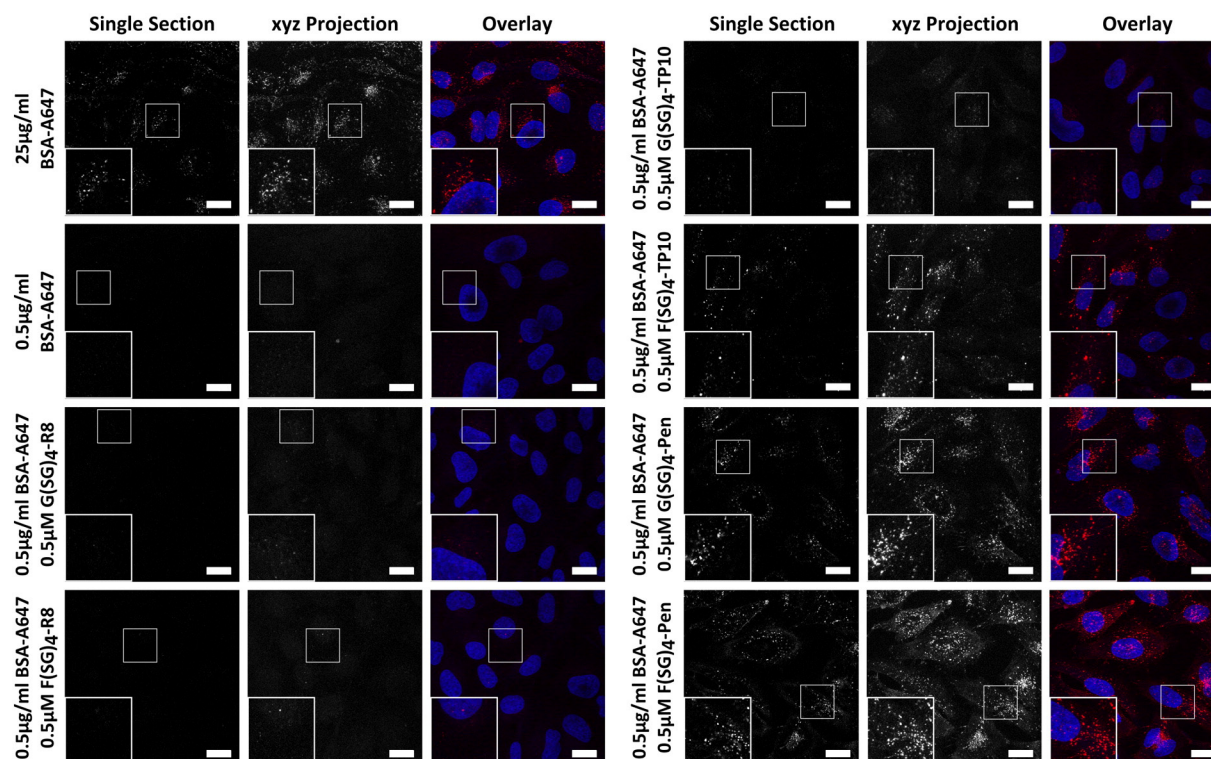


**Fig. 4.** Internalisation of BSA-Alexa647 or BSA-Alexa647-CPP complexes in HeLa Cells. Complexes of 2 µg/ml of BSA-Alexa647 with 2 µM F-/G-(SG)<sub>4</sub>-Penetratin/-R8/-TP10 were allowed to form for 30 min at 37 °C before being diluted 1 in 4 in complete media and incubated with cells for 1 h. Samples were immediately imaged on a confocal microscope with greyscale images showing BSA-Alexa 647 only and overlay images showing BSA-Alexa647 (red) and Hoechst 33342 (blue) as maximum (xyz) projections. Scale bar = 20 µm.

suggested the majority of material was localised to this structure. Cellular labelling demonstrated a dose-dependent increase in integrated fluorescence intensity with increasing Qdot concentration. There was considerable heterogeneity within the sample population with regard

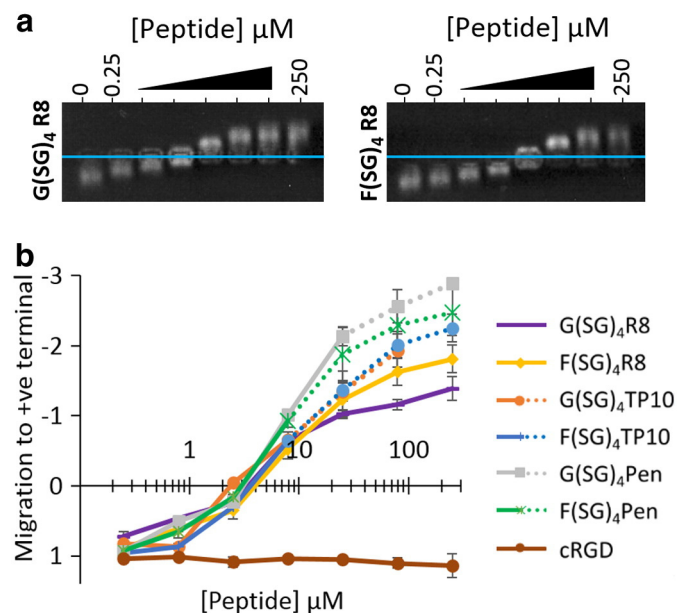


**Fig. 5.** CPP-Qdot complex formation and Qdot uptake in cells. Gly and Phe R8 CPPs (a), and peptides described in Table 1 (b), were assessed for Qdot binding by electrophoresis. Blue lines indicate the position of loading wells. (a) Maximum migratory distance of Qdot bands from the well centre towards the positive electrode was plotted for each peptide and normalised to the Qdot only band. (b) Dotted lines in b indicate well positions in which signs of Qdot aggregation were observed due to the retention of material within the well.

to extent of binding (Supplementary Fig. 6), manifest as larger than expected error bars.

In the presence of a fixed concentration of 1 µM G(SG)<sub>4</sub>R8 or F(SG)<sub>4</sub>R8, cellular binding of Qdots is increased at low and high nanoparticle concentrations (0.316 or 3.16 nM Qdots). In control cells the majority of Qdots appear to localise evenly to the plasma membrane and only a small fraction appear to be internalised in punctate vesicles (Fig. 6a). Complexation of Qdots with Gly or Phe R8 greatly increased Qdot cell binding, with enhanced labelling of both plasma membrane and internal vesicular compartments.

Binding is quantified in Fig. 6b showing that both G(SG)<sub>4</sub>R8 and F(SG)<sub>4</sub>R8 peptides enhance cellular binding of Qdots by roughly 4.8 fold and 9.5 fold respectively, over Qdots alone. Here the Phe modified R8 demonstrated a significant increase in the cell binding activity when compared to the Gly-modified variant. The reasons for this could reflect a direct interaction of the phenylalanine residue with cellular surfaces, or a felicitous display of the peptide at the Qdot surface which enhances cell association via the R8 motif. For penetratin and TP10 Qdots, aggregation was clearly evident making data interpretation problematic. Interestingly the aggregates were only visible on the cell surfaces rather than on the tissue culture plastic (Supplementary Fig. 7).

In light of such a large degree of cargo binding to the plasma membrane we sought to investigate how the constant cycling of plasma membrane components over an extended time frame might affect the internalisation of this membrane associated Qdot fraction. To address this question Qdot complexes were pulsed onto HeLa cells for 1 h followed by a brief counterstain with ConA and a further 24 h recovery (Fig. 6c). Quantification of the integrated intensity per cell revealed that the majority of Qdots at the lower concentration of 0.316 nM were lost during the incubation, with fluorescent profiles only slightly above autofluorescence (Fig. 6b, Supplementary Fig. 8). At 3.16 nM Qdots, control cells also showed little fluorescence, whereas G- and F-(SG)<sub>4</sub>R8 Qdot complexes exhibited binding profiles which paralleled those

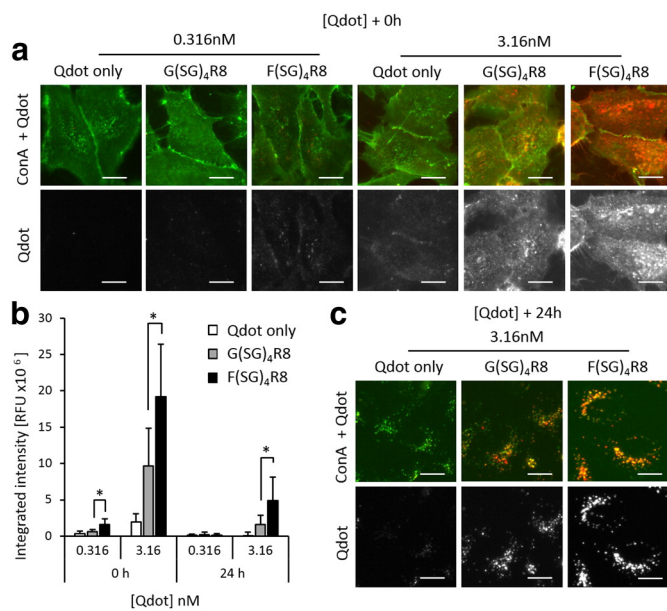


**Fig. 6.** Phe R8 enhances Qdot cell uptake over Gly R8 and Qdots alone. Qdots (red channel) at 0.316 or 3.16 nM (a) were assayed in live HeLa cells for 1 h following complexation with a fixed concentration of 1  $\mu$ M G(SG)<sub>4</sub>R8 or F(SG)<sub>4</sub>R8. ConA-FITC (green channel) was used to label the cell surface allowing Qdot binding to be quantified in (b) by measuring the mean integrated intensity per cell (RFU) in the Qdot channel. After initial loading of Qdot and ConA, cells were reanalysed after a 24 h chase where Qdots redistributed to a perinuclear compartment (c). \*  $p < 0.05$ . Scale bar = 20  $\mu$ m.

recorded after 0 h recovery, although with markedly reduced intensities. By measuring the mean integrated intensity per cell a direct comparison between the two time points was possible, revealing that the Qdot fluorescence remaining after 24 h for 3.16 nM G- and F-(SG)<sub>4</sub>R8 Qdot complexes stood at 17% and 26%, respectively (Fig. 6b). Again, a significantly larger Qdot profile was retained in F-(SG)<sub>4</sub>R8 treated cells when compared to cells incubated with G-(SG)<sub>4</sub>R8. In control cells the majority of ConA was internalised into a perinuclear compartment after 24 h, with Qdots alone showing a reasonable degree of localisation with this probe (Pearson's colocalisation value  $0.54 \pm 0.17$ ). Qdots complexed with Gly or Phe R8 however both showed a striking colocalisation with ConA positive compartments that was more pronounced in the case of Phe-R8 reflecting the increased Qdot cell labelling using this peptide (Pearson's value  $0.71 \pm 0.16$  and  $0.79 \pm 0.12$  for G- and F-(SG)<sub>4</sub>R8 respectively, Fig. 6c). F(SG)<sub>4</sub>R8 complexed Qdots appeared to colocalise almost exclusively with ConA. This lectin has recently received attention due its reported antitumor effects in a variety of cell lines including ML-1<sub>4a</sub> hepatoma [26,27] and MCF-7 breast carcinoma [28] lines. In ML-1<sub>4a</sub> cells, ConA was trafficked to mitochondria and lysosomes following a 3 h incubation triggering LC3-II conversion and cell death [26]. The staining we observed here is consistent with localisation of Qdots and ConA to endolysosomal compartments, indicating Gly and Phe R8 peptides selectively target Qdots to these organelles. As described previously for fluorophore cargo (Fig. 3), cell internalisation during this 24 h period may result primarily as a consequence of plasma membrane turnover opening the possibility of a controlled cell uptake mechanism of nanoparticle, and other CPP cargo, entry. The distribution of material here also bears a strong resemblance to staining by the commercially available Qdot cell label known as Qtracker (Life Technologies) [29]. Qtracker is a labelling kit designed for long-term cell tracking over many generations, and utilises a custom peptide to deliver material to the endolysosomal compartment. We suggest that using non-covalent binding of R8 peptides to amine Qdots may be a viable alternative for cell tracking experiments, and opens the possibility of extending this method to other nanoparticles of interest.

## 4. Conclusions

Here we have demonstrated the ability of a single Gly to Phe change in the N-terminus of a neutral bridging sequence to have a dramatic change in the uptake and delivery capacity of three different CPPs. In some cases this significantly enhances the vector properties of the CPP. The universality of this strategy of adding a hydrophobic entity downstream or possibly upstream of the CPP sequence remains to be determined.

## Acknowledgements

KC is funded through a Cardiff University Presidents Research scholarship and an EPSRC Cross-Disciplinary Interfaces Programme (EP/I016260/1). Funding from: Cardiff University Partnership Fund (ATJ, ES), EPSRC Grant EP/J021334/1 (PW, ATJ, ES) and Egyptian Ministry of Higher Education (NGE, ATJ) is also acknowledged.

## Appendix A. Supplementary data

Supplementary data to this article can be found online at <http://dx.doi.org/10.1016/j.jconrel.2014.07.055>.

## References

- [1] M. Mae, U. Langel, Cell-penetrating peptides as vectors for peptide, protein and oligonucleotide delivery, *Curr. Opin. Pharmacol.* 6 (2006) 509–514.
- [2] D.S. Youngblood, S.A. Hatlevig, J.N. Hassinger, P.L. Iversen, H.M. Moulton, Stability of cell-penetrating peptide-morpholino oligomer conjugates in human serum and in cells, *Bioconjug. Chem.* 18 (2007) 50–60.
- [3] E. Carter, C.Y. Lau, D. Tosh, S.G. Ward, R.J. Mersny, Cell penetrating peptides fail to induce an innate immune response in epithelial cells *in vitro*: implications for continued therapeutic use, *Eur. J. Pharm. Biopharm.* 85 (2013) 12–19.
- [4] el-S. Khafagy, M. Morishita, N. Ida, R. Nishio, K. Isowa, K. Takayama, Structural requirements of penetratin absorption enhancement efficiency for insulin delivery, *J. Control. Release* 143 (2010) 302–310.
- [5] K. Cleal, L. He, P.D. Watson, A.T. Jones, Endocytosis, intracellular traffic and fate of cell penetrating peptide based conjugates and nanoparticles, *Curr. Pharm. Des.* 19 (2013) 2878–2894.
- [6] F.C. Chien, C.W. Kuo, P. Chen, Localization imaging using blinking quantum dots, *Analyst* 136 (2011) 1608–1613.
- [7] F. Pinaud, S. Clarke, A. Sittner, M. Dahan, Probing cellular events, one quantum dot at a time, *Nat. Methods* 7 (2010) 275–285.
- [8] E. Petryayeva, W.R. Algar, I.L. Medintz, Quantum dots in bioanalysis: a review of applications across various platforms for fluorescence spectroscopy and imaging, *Appl. Spectrosc.* 67 (2013) 215–252.
- [9] B.R. Liu, Y.W. Huang, J.G. Winiarz, H.J. Chiang, H.J. Lee, Intracellular delivery of quantum dots mediated by a histidine- and arginine-rich HR9 cell-penetrating peptide through the direct membrane translocation mechanism, *Biomaterials* 32 (2011) 3520–3537.
- [10] A.T. Jones, E.J. Sayers, Cell entry of cell penetrating peptides: tales of tails wagging dogs, *J. Control. Release* 161 (2012) 582–591.
- [11] C.L. Watkins, E.J. Sayers, C. Allender, D. Barrow, C. Fegan, P. Brennan, A.T. Jones, Co-operative membrane disruption between cell-penetrating peptide and cargo: implications for the therapeutic use of the Bcl-2 converter peptide D-NuBCP-9-r8, *Mol. Ther.* 19 (2011) 2124–2132.
- [12] V.P. Reddy Chichili, V. Kumar, J. Sivaraman, Linkers in the structural biology of protein–protein interactions, *Protein Sci.* 22 (2013) 153–167.
- [13] C.L. Watkins, D. Schmaljohann, S. Futaki, A.T. Jones, Low concentration thresholds of plasma membranes for rapid energy-independent translocation of a cell-penetrating peptide, *Biochem. J.* 420 (2009) 179–189.
- [14] C.A. Schneider, W.S. Rasband, K.W. Eliceiri, NIH Image to ImageJ: 25 years of image analysis, *Nat. Methods* 9 (2012) 671–675.
- [15] C.L. Watkins, P. Brennan, C. Fegan, K. Takayama, I. Nakase, S. Futaki, A.T. Jones, Cellular uptake, distribution and cytotoxicity of the hydrophobic cell penetrating peptide sequence PFVYLI linked to the proapoptotic domain peptide PAD, *J. Control. Release* 140 (2009) 237–244.
- [16] M.M. Fretz, N.A. Penning, S. Al-Taei, S. Futaki, T. Takeuchi, I. Nakase, G. Storm, A.T. Jones, Temperature-, concentration- and cholesterol-dependent translocation of L- and D-octa-arginine across the plasma and nuclear membrane of CD34+ leukaemia cells, *Biochem. J.* 403 (2007) 335–342.
- [17] K. Takayama, H. Hirose, G. Tanaka, S. Pujals, S. Katayama, I. Nakase, S. Futaki, Effect of the attachment of a penetration accelerating sequence and the influence of hydrophobicity on octaarginine-mediated intracellular delivery, *Mol. Pharm.* 9 (2012) 1222–1230.
- [18] K. Takayama, I. Nakase, H. Michiue, T. Takeuchi, K. Tomizawa, H. Matsui, S. Futaki, Enhanced intracellular delivery using arginine-rich peptides by the addition of penetration accelerating sequences (Pas), *J. Control. Release* 138 (2009) 128–133.

- [19] J.A. Killian, G. von Heijne, How proteins adapt to a membrane–water interface, *Trends Biochem. Sci.* 25 (2000) 429–434.
- [20] Z.G. Peng, K. Hidajat, M.S. Uddin, Selective and sequential adsorption of bovine serum albumin and lysozyme from a binary mixture on nanosized magnetic particles, *J. Colloid Interface Sci.* 281 (2005) 11–17.
- [21] S. Aubry, F. Burlina, E. Dupont, D. Delaroche, A. Joliot, S. Lavielle, G. Chassaing, S. Sagan, Cell-surface thiols affect cell entry of disulfide-conjugated peptides, *FASEB J.* 23 (2009) 2956–2967.
- [22] H. Yukawa, M. Watanabe, N. Kaji, Y. Okamoto, M. Tokeshi, Y. Miyamoto, H. Noguchi, Y. Baba, S. Hayashi, Monitoring transplanted adipose tissue-derived stem cells combined with heparin in the liver by fluorescence imaging using quantum dots, *Biomaterials* 33 (2012) 2177–2186.
- [23] B.R. Liu, J.S. Liou, Y.W. Huang, R.S. Aronstam, H.J. Lee, Intracellular delivery of nanoparticles and DNAs by IR9 cell-penetrating peptides, *PLoS One* 8 (2013) e64205.
- [24] G.R. Dakwar, E. Zagato, J. Delanghe, S. Hobel, A. Aigner, H. Denys, K. Braeckmans, W. Ceelen, S.C. De Smedt, K. Remaut, Colloidal stability of nano-sized particles in the peritoneal fluid: towards optimizing drug delivery systems for intraperitoneal therapy, *Acta Biomater.* 10 (7) (2014) 2965–2975.
- [25] R.C. Van Lehn, A. Alexander-Katz, Ligand-mediated short-range attraction drives aggregation of charged monolayer-protected gold nanoparticles, *Langmuir* 29 (2013) 8788–8798.
- [26] H.Y. Lei, C.P. Chang, Lectin of Concanavalin A as an anti-hepatoma therapeutic agent, *J. Biomed. Sci.* 16 (2009) 10.
- [27] C.P. Chang, M.C. Yang, H.S. Liu, Y.S. Lin, H.Y. Lei, Concanavalin A induces autophagy in hepatoma cells and has a therapeutic effect in a murine *in situ* hepatoma model, *Hepatology* 45 (2007) 286–296.
- [28] Z. Shi, J. Chen, C.Y. Li, N. An, Z.J. Wang, S.L. Yang, K.F. Huang, J.K. Bao, Antitumor effects of concanavalin A and *Sophora flavescens* lectin *in vitro* and *in vivo*, *Acta Pharmacol. Sin.* 35 (2014) 248–256.
- [29] B.C. Lagerholm, M. Wang, L.A. Ernst, D.H. Ly, H. Liu, M.P. Bruchez, A.S. Waggoner, Multicolor coding of cells with cationic peptide coated quantum dots, *Nano Lett.* 4 (2004) 2019–2022.